Volume 287 Issue 2 25 January 2006 ISSN 0022-0248

ELSEVIER

JOURNAL OF CRYSTAL GROWTH

Editors: T.F. KUECH (Principal Editor)
M. SCHIEBER (Founding Editor)
R.S. FEIGELSON, R. KERN,
K. NAKAJIMA, G.B. STRINGFELLOW

The 16th American Conference on Crystal Growth & Epitaxy and The 12th Biennial Workshop on OMVPE

ACCGE-16
July 10–15, 2005

Guest Editors:
M. Skowronski,
P.G. Schunemann,
J.J. Derby

OMVPE-12
July 10–14, 2005

Guest Editors:
R. Bhat,
C. Caneau

LINDA HALL
FEB 07 2006
LIBRARY

LAST ISSUE OF THIS VOLUME

Also available on
SCIENCE DIRECT®
www.sciencedirect.com

Journal of Crystal Growth

http://www.elsevier.com/locate/jcrysgro

Scope of the journal: Experimental and theoretical contributions are invited in the following fields: Theory of nucleation and growth, molecular kinetics and transport phenomena, crystallization in viscous media such as polymers and glasses. Crystal growth of metals, minerals, semiconductors, magnetics, inorganic, organic and biological substances in bulk or as thin films. Apparatus, instrumentation and techniques for crystal growth, and purification methods. Characterization of single crystals by physical and chemical methods.

EDITORIAL BOARD

T.F. KUECH (Principal Editor)
Dept. of Chemical Engineering, University of Wisconsin-Madison, Madison, WI 53706, USA
Fax: +1 608 265 3782; e-mail: kuech@engr.wisc.edu

M. SCHIEBER (Founding Editor)
The Fredy and Nadine Herrmann Graduate School of Applied Science, Hebrew University, Jerusalem 91904, Israel
Fax: +972 2 566 3878; e-mail: schieber@vms.huji.ac.il

R.S. FEIGELSON
Geballe Laboratory for Advanced Materials, McCullough Building, 476 Lomita Mall, Stanford University, Stanford, CA 94305-4045, USA
Tel.: +1 650 723 4007; fax: +1 650 723 3752;
E-mail: feigel@soe.stanford.edu

R. KERN
CRMCN, CNRS, Campus de Luminy, Case 913,
F-13288 Marseille Cedex 9, France
Fax: +33 4 91 418 916; e-mail: kern@crmcn.univ-mrs.fr

K. NAKAJ IMA
Institute of Materials Research, Tohoku University,
Katahira 2-1-1, Sendai 980-8577, Japan
Fax: +81 22 215 2011; e-mail: nakajima@imr.tohoku.ac.jp

G.B. STRINGFELLOW
Electrical and Computer Engrg. Dept., University of Utah,
50 S.Central Campus Drive, 3280 MEB, Salt Lake City, UT 84112, USA
E-mail: stringfellow@eng.utah.edu

ASSOCIATE EDITORS

H. Asahi
Tel.: +81 6 6879 840; Fax: +81 6 6879 8409; e-mail: asahi@sanken.osaka-u.ac.jp

K.W. BENZ (Microgravity, Electronic materials)
Fax: +49 761 203 4709; e-mail:Klaus-werner.benz@fmf.uni-freiburg.de

R. BHAT (Thin film, Epitaxial growth)
Fax: +1 607 974 1650; Tel.: +1 607 974 1035; e-mail bhatr@corning.com

R.M. BIEFELD (Epitaxial growth and nanostructures)
Fax: +1 505 844 3211; e-mail rmbiefe@sandia.gov

N.E. CHAYEN (Crystallization of biological macromolecules)
Fax: +44 171 594 3169; e-mail: n.chayen@ic.ac.uk

A.A. CHERNOV (Kinetics of Crystallization, Protein crystallization)
Fax: +1 256 544 2102; tel.: +1 256 544 9196; e-mail: alex.chernov@msfc.nasa.gov

J.J. DERBY (Computational models)
Fax: +1 612 626 7246; e-mail: derby@umn.edu

R. FORNARI (Substrates, Growth from the melt, MO Chemical vapour deposit, Oxides,
Fax.: +49 30 6392 3003; e-mail fornari@ikz-berlin.de

V. FRATELLO (Oxide crystals, Liquid phase epitaxy of oxides, Solution growth of oxides, Magnetic materials, Optical materials)
Fax: +1 908 281 0191; e-mail: vjfratello@integratedphotonics.com

M.E. GLICKSMAN (Solidification)
Fax: +1 518 276 2198; e-mail: glickm@rpi.edu

M.S. GOORSKY (XRD characterization, Epitaxy for devices)
Fax: +1 310 206 7353; e-mail: goorsky@seas.ucla.edu

T. HIBIYA (Oxides, Melt, Thermophysical properties, Microgravity)
Tel.: +81 42 585 8654; e-mail: hibiya@cc.tmit.ac.jp

R. JAMES (II–VI semiconductors, Radiation sensors)
Fax: +1 631 344 5584; e-mail: rjames@bnl.gov

M. KAWASAKI (Oxide thin films and epitaxy)
Fax: +81 22 215 2086; e-mail: kawasaki@imr.tohoku.ac.jp

B.A. KORGEL (Nanocrystals, Nanowires)
Fax: +1 512 471 7060; tel.: +1 512 471 5633; e-mail: korgel@che.utexas.edu

K.M. LAU
Tel.: +852 235 870 49; e-mail: eekmlau@ust.hk

G.B. McFADDEN (Theory)
Fax: +1 301 990 4127; e-mail: mcfadden@nist.gov

J.B. MULLIN (Semiconductors)
Fax: +44 1202 759 835; e-mail: brian.mullin@btinternet.com

D.N. NORTON (Oxide thin films and epitaxy)
Fax: +1 352 846 1182; e-mail: dnort@mse.u.edu

K.H. PLOOG (Molecular beam epitaxy)
Fax: +49 30 203 77201; e-mail: ploog@pdi-berlin.de

J.M. REDWING (Nanoscale Materials, Quantum Dots, Nanoparticles, Nanowires)
Tel.: +1 814 865 8665; e-mail: redwing@matse.psu.edu

M. ROTH (Nonlinear optical and electro-optical materials)
Fax: +972 2 566 3878; e-mail: mroth@vms.huji.ac.il

P. RUDOLPH (Defects, Bulk growth, Special types of growth technologies, Semiconductors,
Fax: +49 30 6392 3003; e-mail: Rudolph@ikz-berlin.de

K. SATO (Biocrystallization and organic crystals)
Fax: +81 824 227 062; e-mail: kyosato@hiroshima-u.ac.jp

D.W. SHAW (Semiconductors, Epitaxy, Devices)
Fax: +1 972 883-6839; e-mail: dshaw@utdallas.edu

S. UDA (Oxide crystal growth, Physical chemistry of melt, Growth mechanism)
Fax.: +81 22 215 2101; e-mail: uda@imr.tohoku.ac.jp

M. UWAHA (Growth kinetics)
Fax: +81 52 789 2928; e-mail: uwaha@phys.nagoya-u.ac.jp

S. VEESLER (Solution growth: industrial; biological macromolecules; pharmaceutical compounds)
Fax: +33 04 91 41 89; tel: +33 06 62 92 28; e-mail: veesler@cmcn.univ.mrs.fr

P.G. VEKILOV (Nucleation theory, Solution growth mechanisms, Protein crystallization)
Fax: +1 713 743 4323; tel: +1 713 743 4315; e-mail: vekilov@uh.edu

Abstracted/indexed in
Aluminium Industry Abstracts; Chemical Abstracts; Current Contents: Physical, Chemical and Earth Sciences; EI Compendex Plus; Engineered Materials Abstracts; Engineering Index; INSPEC; Metals Abstracts

Publication information Journal of Crystal Growth (ISSN 0022-0248). For 2006, volume(s) 286–297 are scheduled for publication. Subscription prices are available upon request from the Publisher or from the Regional Sales Office nearest you or from this journal's website (http://www.elsevier.com/locate/jcrysgro).Further information is available on this journal and other Elsevier products through Elsevier's website (http://www.elsevier.com). Subscriptions are accepted on a prepaid basis only and are entered on a calendar year basis. Issues are sent by standard mail (surface within Europe, air delivery outside Europe). Priority rates are available upon request. Claims for missing issues should be made within six months of the date of dispatch.

USA mailing notice: Journal of Crystal Growth (ISSN 0022-0248) is published semimonthly by Elsevier (P.O. Box 211, 1000 AE Amsterdam, The Netherlands). Annual subscription price in the USA is US$ 11.109 (valid in North, Central and South America), including air speed delivery. Periodical postage rate paid at Jamaica, NY 11431.

USA POSTMASTER: Send address changes to Journal of Crystal Growth, Publications Expediting Inc., 200 Meacham Ave, Elmont, NY 11003.
AIRFREIGHT AND MAILING in the USA by Publications Expediting Inc., 200 Meacham Avenue, Elmont, NY 11003.

Printed in the Netherlands

JOURNAL OF CRYSTAL GROWTH

VOLUME 287 (2006)

LINDA HALL
FEB 07 2006
LIBRARY

© 2006 Elsevier B.V. All rights reserved

This journal and the individual contributions contained in it are protected under copyright by Elsevier B.V., and the following terms and conditions apply to their use:

Photocopying

Single photocopies of single articles may be made for personal use as allowed by national copyright laws. Permission of the Publisher and payment of a fee is required for all other photocopying, including multiple or systematic copying, copying for advertising or promotional purposes, resale, and all forms of document delivery. Special rates are available for educational institutions that wish to make photocopies for non-profit educational classroom use.

Permissions may be sought directly from Elsevier's Rights Department in Oxford, UK: phone (+44)1865843830, fax (+44)1865853333, e-mail permissions@elsevier.com. Requests may also be completed on-line via the Elsevier homepage (http://www.elsevier.com/locate/permissions).

In the USA, users may clear permissions and make payments through the Copyright Clearing Center, Inc., 222 Rose Wood Drive, Danvers, MA 01923, USA; phone: (+1) (978) 7508400, fax: (+1) (978) 7504744, and in the UK through the Copyright Licensing Agency Rapid Clearance Service (CLARCS), 90 Tottenham Court Road, London W1P 0LP, UK; phone: (+44) 20 7631 5555, fax: (+44) 20 7631 5500. Other countries may have a local reprographic rights agency for payments.

Derivative works

Subscribers may reproduce tables of contents or prepare lists of articles including abstracts for internal circulation within their institutions. Permission of the Publisher is required for resale or distribution outside the institution.

Permission of the Publisher is required for all other derivative works, including compilations and translations.

Electronic storage or usage

Permission of the Publisher is required to store or use electronically any material contained in this journal, including any article or part of an article.

Except as outlined above, no part of this publication may be reproduced, stored in a retrieval system or transmitted in any form or by any means, electronic, mechanical, photocopying, recording or otherwise, without prior written permission of the Publisher.

Address permissions requests to: Elsevier Rights Department, at the fax and e-mail addresses noted above.

Notice

No responsibility is assumed by the Publisher for any injury and/or damage to persons or property as a matter of products liability, negligence or other wise, or from any use or operation of any methods, products, instructions or ideas contained in the material herein. Because of rapid advances in the medical sciences, in particular, independent verification of diagnoses and drug dosages should be made.

Although all advertising material is expected to conform to ethical (medical) standards, inclusion in this publication does not constitute a guarantee or endorsement of the quality of such product or of the claims made of it by its manufacturer.

Orders, claims, and Journal enquiries: please contact the Customer Service Department at the Regional Sales Office nearest you:

Orlando: Elsevier, Customer Service Department, 6277 Sea Harbor Drive, Orlando, FL 32887-4800, USA; phone: (+1)(877)8397126 [toll free number for US customers], or (+1)(407)3454020 [customers outside US]; fax: (+1)(407)3631354; e-mail: usjcs@elsevier.com.

Amsterdam: Elsevier, Customer Service Department, PO Box 211, 1000 AE Amsterdam, The Netherlands; phone: (+31)(20)4853757; fax: (+31)(20)4853432; e-mail: nlinfo-f@elsevier.com.

Tokyo: Elsevier, Customer Service Department, 4F Higashi-Azabu, 1-Chome Bldg, 1-9-15 Higashi-Azabu, Minato-ku, Tokyo 106-0044, Japan; phone: (+81)(3)55615037; fax: (+81)(3)5561 5047; e-mail: jp.info@elsevier.com.

Singapore: Elsevier, Customer Service Department, 3 Killiney Road, #08-01 Winsland House I, Singapore 239519; phone: (+65)63490222; fax: (+65)67331510; e-mail: asiainfo@elsevier.com.

Author enquiries

Submissions

For enquiries relating to the submission of articles (including electronic submission where available) please visit Elsevier's Author Gateway at http://authors.elsevier.com. The Author Gateway also provides the facility to track accepted articles and set up e-mail alerts to inform you of when an article's status has changed, as well as detailed artwork guidelines, copyright information, frequently asked questions and more.

Contact details for questions arising after acceptance of an article, especially those relating to proofs, are provided after registration of an article for publication.

Other enquiries

Visit Elsevier's Author Gateway (http://authors.elsevier.com) for the facility to track accepted articles and set up e-mail alerts to inform you of when an article's status has changed. The Author Gateway also provides detailed artwork guidelines, copyright information, frequently asked questions and more. Contact details for questions arising after acceptance of an article, especially those relating to proofs, are provided after registration of an article for publication.

Language Polishing: For authors who require information about language editing and copyedititng services pre- and post- submission please visit http://www.elsevier.com/wps/find/authorshome.authors/languagepolishing or contact authorsupport@elsvier.com for more information. Please note Elsevier neither endorses nor takes responsibility for any products, goods or services offered by outside vendors through our services or in any advertising. For more information please refer to our Terms & Conditions http://www,elsevier.com/wps/find/termsconditions.cws.home/termsconditions.

Advertising information

Advertising orders and enquiries can be sent to: **South America**: Mr Tino DeCarlo, The Advertising Department, Elsevier Inc., 360 Park Avenue South, New York, NY 10010-1710, USA; phone.: (+1) (212) 633 3815; fax: (+1) (212) 633 3820; e-mail: t.decarlo@elsevier.com. **Japan**: The Advertising Department, Elsevier K.K., 4F Higashi-Azabu, 1-Chome Bldg., 1-9-15 Higashi-Azabu, Minato-ku, Tokyo 106-0044, Japan; tel.: (+81) (3) 5561 5037; fax: (+81) (3) 5561 5047; e-mail: jp.info@elsevier.com. **Canada, Europe, USA and the rest of the World**: Miss Katrina Barton, tel.: (+44) (0) 20 7611 4117; fax: (+44) (0) 20 7611 4463; e-mail: commercialsales@elsevier.com.

♾ The paper used in this publication meets the requirements of ANSI/NISO Z39.48-1992 (Permanence of Paper)

The 16th American Conference on Crystal Growth & Epitaxy and The 12th Biennial Workshop on OMVPE

ACCGE-16
July 10–15, 2005

OMVPE-12
July 10–14, 2005

Guest Editors:
M. Skowronski,
P.G. Schunemann,
J.J. Derby

Guest Editors:
R. Bhat,
C. Caneau

ELSEVIER
Amsterdam – Boston – Jena – London – New York – Oxford – Paris
Philadelphia – San Diego – St. Louis

Contents

The 16th American Conference on Crystal Growth & Epitaxy and The 12th Biennial Workshop on OMVPE

ACCGE-16
July 10–15, 2005

OMVPE-12
July 10–14, 2005

Preface
M. Skowronski, P.G. Schunemann and J.J. Derby 213

Section 1: Bulk Crystal Growth

Theoretical and technological solutions of the striation problem
H.J. Scheel 214

Growth of $Ga_{(1-x)}In_xSb$ alloys by Vertical Bridgman technique under alternating magnetic field
A. Mitric, T. Duffar, C. Diaz-Guerra, V. Corregidor, L.C. Alves, C. Garnier and G. Vian 224

Crystal growth and optical properties of Dy-doped potassium lead bromide (KPb_2Br_5)
U. Hömmerich, E. Nyein, J.A. Freeman, P. Amedzake, S.B. Trivedi and J.M. Zavada 230

Dielectric spectrum of rare-earth-doped calcium fluoride crystals
I. Nicoara, M. Munteanu, N. Pecingina-Girjioaba, M. Stef and L. Lighezan 234

Bridgman growth of $LaBr_3$:Ce and $LaCl_3$:Ce crystals for high-resolution gamma-ray spectrometers
W.M. Higgins, J. Glodo, E. Van Loef, M. Klugerman, T. Gupta, L. Cirignano, P. Wong and K.S. Shah 239

Crystal growth and infrared spectroscopy of Cr:$Cd_{1-x}Zn_xTe$ and Cr:$Cd_{1-x}Mg_xTe$
U. Hömmerich, A.G. Bluiett, I.K. Jones, S.B. Trivedi and R.T. Shah 243

Horizontal gradient freeze growth of $AgGaGeS_4$ and $AgGaGe_5Se_{12}$
P.G. Schunemann, K.T. Zawilski and T.M. Pollak 248

Solidification interface shape control in a continuous Czochralski silicon growth system
C. Wang, H. Zhang, T. Wang and L. Zheng 252

Quality evaluation of resistivity-controlled silicon crystals
J.H. Wang 258

Growth of oriented tricrystals of an Fe–Si alloy
P. Lejček, J. Kopeček and M. Jarošová 262

Preferential growth direction in Fe-28 at.%Al-4 at.%Cr alloy
J. Kopeček and P. Lejček 267

Comparing modified vertical gradient freezing with rotating magnetic fields or with steady magnetic and electric fields
X. Wang, N. Ma, D.F. Bliss, G.W. Iseler and P. Becla 270

3D unsteady analysis of gas turbulent convection during HPLEC InP growth
E.N. Bystrova and V.V. Kalaev 275

0022-0248/$-see front matter
doi:10.1016/S0022-0248(05)01641-6

Numerical investigation of crucible rotation effect on crystallization rate behavior during Czochralski growth of $Si_{1-x}Ge_x$ crystals
O.V. Smirnova, V.V. Kalaev, Yu.N. Makarov, N.V. Abrosimov and H. Riemann 281

3D mass diffusivity model of liquid metals in the presence of a magnetic field
Y.Y. Khine and R.M. Banish 287

Section 2: Growth and Properties of Oxides

Voids engulfment in shaped sapphire crystals
I. Nicoara, O.M. Bunoiu and D. Vizman 291

Growth of 3-inch diameter near-stoichiometric $LiTaO_3$ by conventional Czochralski technique
D.P. Shumov, J. Rottenberg and S. Samuelson 296

The Czochralski growth of large-diameter $La_3Ga_{5.5}Ta_{0.5}O_{14}$ crystals along different orientations
J. Luo, D. Shah, C.F. Klemenz, M. Dudley and H. Chen 300

Synthesis and characterization of solid solutions in $ABCO_4$ system
A. Novoselov, G. Zimina, L. Komissarova and A. Pajaczkowska 305

Study on crystal growth and luminescence properties of Pr-doped RE_2SiO_5 (RE = Y, Lu)
A. Novoselov, H. Ogino, A. Yoshikawa, M. Nikl, J. Pejchal, J.A. Mares, A. Beitlerova, C. D'Ambrosio and T. Fukuda 309

Crystal growth and optical absorption of pure and Ti, Mn-doped $MgAl_2O_4$ spinel
A. Jouini, H. Sato, A. Yoshikawa, T. Fukuda, G. Boulon, K. Kato and E. Hanamura 313

Single-crystal growth and superconductivity of $(La_{1-x}Sr_x)_2CaCu_2O_{6+\delta}$
G.D. Gu, M. Hucker, Y.-J. Kim, J.M. Tranquada, Q. Li and A.R. Moodenbaugh 318

Growth of alkaline-earth vanadate garnet by synthetic contact metamorphism with molten V_2O_5–Na_2SiO_3 acting on dolomite
T.F. Ciszek 323

Synthesis, phase segregation and properties of piezo-/ferroelectric $(1-x)Pb(Sc_{1/2}Nb_{1/2})O_3$–$xPbTiO_3$ single crystals
Y.-H. Bing and Z.-G. Ye 326

3D numerical simulation of heat transfer during horizontal direct crystallization of corundum single crystals
M.A. Lukanina, K.V. Hodosevitch, V.V. Kalaev, V.B. Semenov, V.N. Sytin and V.L. Raevsky 330

Growth and scintillation properties of Pr-doped $Lu_3Al_5O_{12}$ crystals
H. Ogino, A. Yoshikawa, M. Nikl, A. Krasnikov, K. Kamada and T. Fukuda 335

Section 3: Wide Band Gap Semiconductors

Effects of hydrogen on the properties of SiC crystals grown by physical vapor transport: Thermodynamic considerations and experimental results
M.A. Fanton, Q. Li, A.Y. Polyakov, M. Skowronski, R. Cavalero and R. Ray 339

Epitaxial growth and characterization of silicon carbide films
G. Dhanaraj, M. Dudley, Y. Chen, B. Ragothamachar, B. Wu and H. Zhang 344

Characterization of bulk grown GaN and AlN single crystal materials
B. Raghothamachar, J. Bai, M. Dudley, R. Dalmau, D. Zhuang, Z. Herro, R. Schlesser, Z. Sitar, B. Wang, M. Callahan, K. Rakes, P. Konkapaka and M. Spencer 349

Study of carrier localization in InGaN/GaN quantum well blue-light-emitting diode structures
J.H. Chen, Z.C. Feng, J.C. Wang, H.L. Tsai, J.R. Yang, A. Parekh, E. Armour and P. Faniano 354

Growth of nitrogen-doped SiC boules by halide chemical vapor deposition
M. Fanton, D. Snyder, B. Weiland, R. Cavalero, A. Polyakov, M. Skowronski and H. Chung 359

Growth of 6H-SiC crystals with low boron concentration
M.A. Fanton, R.L. Cavalero, B.E. Weiland, R.G. Ray, D.W. Snyder, R.D. Gamble, E.J. Oslosky and W.J. Everson 363

Fabrication of homoepitaxial ZnO films by low-temperature liquid-phase epitaxy
D. Ehrentraut, H. Sato, M. Miyamoto, T. Fukuda, M. Nikl, K. Maeda and I. Niikura 367

Seeded growth of AlN single crystals by physical vapor transport
D. Zhuang, Z.G. Herro, R. Schlesser and Z. Sitar 372

Ammonothermal growth of GaN crystals in alkaline solutions
B. Wang, M.J. Callahan, K.D. Rakes, L.O. Bouthillette, S.-Q. Wang, D.F. Bliss and J.W. Kolis 376

Hydrothermal growth and characterization of nitrogen-doped ZnO crystals
B. Wang, M.J. Callahan, L.O. Bouthillette, C. Xu and M.J. Suscavage 381

Section 4: Materials for Photovoltaics

Progress with polycrystalline silicon thin-film solar cells on glass at UNSW
A.G. Aberle 386

High-throughput zone-melting recrystallization for crystalline silicon thin-film solar cells
S. Reber, A. Eyer and F. Haas 391

Laser crystallization — a way to produce crystalline silicon films on glass or on polymer substrates
F. Falk and G. Andrä 397

Transition metals in photovoltaic-grade ingot-cast multicrystalline silicon: Assessing the role of impurities in silicon nitride crucible lining material
T. Buonassisi, A.A. Istratov, M.D. Pickett, J.-P. Rakotoniaina, O. Breitenstein, M.A. Marcus, S.M. Heald and E.R. Weber 402

Kinetics of the reactive crystallization of $CuInSe_2$ and $CuGaSe_2$ chalcopyrite films for solar cell applications
M. Purwins, A. Weber, P. Berwian, G. Müller, F. Hergert, S. Jost and R. Hock 408

Low-temperature silicon homoepitaxy by hot-wire chemical vapor deposition with a Ta filament
C.W. Teplin, Q. Wang, E. Iwaniczko, K.M. Jones, M. Al-Jassim, R.C. Reedy and H.M. Branz 414

Pocket surface and slip defect in Si epitaxy
T.Y. Wang and D.J. Carlson 419

A simple model explaining the preferential (1 0 0) orientation of silicon thin films made by aluminum-induced layer exchange
J. Schneider, A. Sarikov, J. Klein, M. Muske, I. Sieber, T. Quinn, H.S. Reehal, S. Gall and W. Fuhs 423

Large silicon crystal hollow-tube growth by the edge-defined film-fed growth (EFG) method
B. Mackintosh, A. Seidl, M. Ouellette, B. Bathey, D. Yates and J. Kalejs 428

Extended defects in Si films epitaxially grown by low-temperature ECRCVD
B. Rau, K. Petter, I. Sieber, M. Stöger-Pollach, D. Eyidi, P. Schattschneider, S. Gall, K. Lips and W. Fuhs 433

Progress in epitaxial deposition on low-cost substrates for thin-film crystalline silicon solar cells at IMEC
K.V. Nieuwenhuysen, F. Duerinckx, I. Kuzma, D.v. Gestel, G. Beaucarne and J. Poortmans 438

Theoretical study of the initial stage of the aluminium-induced layer-exchange process
A. Sarikov, J. Schneider, J. Klein, M. Muske and S. Gall 442

Kinetics of SiGe chemical vapor deposition from chloride precursors
A.A. Lovtsus, A.S. Segal, A.P. Sid'ko, R.A. Talalaev, P. Storck and L. Kadinski 446

Section 5: Characterization

Comparison of the optical properties of diffusion-doped polycrystalline Cr:ZnSe and Cr:CdTe windows
U. Hömmerich, I.K. Jones, E. Ei Nyein and S.B. Trivedi 450

Electric-field poling effect on thermal stability of monoclinic phase in $Pb(Mg_{1/3}Nb_{2/3})_{0.74}Ti_{0.26}O_3$ single crystal
R.R. Chien, V.H. Schmidt and C.-S. Tu 454

Influence of annealing temperature on the grain growth of samarium-doped ceria
H.-H. Huang, H.-P. Chang, Y.-T. Chien, M.-C. Huang and J.-S. Wang 458

Single domain structure and two-color holographic recording in $LiNbO_3$:Cu:Ce crystals grown by the vertical Bridgman method
X. Liang, X. Xu, T.-C. Chong, M. Li and S. Solanki 463

Characterization of Berthelot-type behaviors of InGaN/GaN semiconductor heterosystems
T.-E. Nee, H.-T. Shen, J.-C. Wang and R.-M. Lin 468

SIMS-depth profile and microstructure studies of Ti-diffused Mg-doped near-stoichiometric lithium niobate waveguide
R.M. Kumar, F. Yamamoto, J. Ichikawa, H. Ryoken, I. Sakaguchi, X. Liu, M. Nakamura, K. Terabe, S. Takekawa, H. Haneda and K. Kitamura 472

Laser-induced damage mechanisms and improvement of optical qualities of bulk potassium dihydrogen phosphate crystals
K. Wang, C. Fang, J. Zhang, X. Sun, S. Wang, Q. Gu, X. Zhao and B. Wang 478

Structural modulation in bismuth cuprate superconductor observed by X-ray reciprocal space mapping
S. Kaneko, K. Akiyama, Y. Shimizu, Y. Hirabayashi, S. Ohya, H. Funakubo and M. Yoshimoto 483

Section 6: Fundamentals

The phase-field theory applied to CO_2 and CH_4 hydrate
A. Svandal, B. Kvamme, L. Gránásy, T. Pusztai, T. Buanes and J. Hove 486

Computer simulation of CO_2 hydrate growth
T. Buanes, B. Kvamme and A. Svandal 491

Section 7: Nano- and Bio-Crystallization

Two-dimensional phase-field simulation of self-assembled quantum dot formation
T. Takaki, T. Hasebe and Y. Tomita 495

Molecular beam epitaxial growth of high-quality GaN nanocolumns
J.E. Van Nostrand, K.L. Averett, R. Cortez, J. Boeckl, C.E. Stutz, N.A. Sanford, A.V. Davydov and J.D. Albrecht 500

Growth and characterization of defect free GaAs nanowires
B.A. Wacaser, K. Deppert, L.S. Karlsson, L. Samuelson and W. Seifert 504

Growth of highly ordered relaxed InAs/GaAs quantum dots on non-lithographically patterned substrates by molecular beam epitaxy
W. Guo, R.S. Guico, R. Beresford and J.M. Xu 509

Aligned Co nanodiscs by electrodeposition on GaAs
Z. Liang Bao and K.L. Kavanagh 514

Morphological evolution of Ge islands on Au-patterned Si
J.T. Robinson, J.A. Liddle, A. Minor, V. Radmilovic and O.D. Dubon 518

Spontaneously grown GaN and AlGaN nanowires
K.A. Bertness, A. Roshko, N.A. Sanford, J.M. Barker and A.V. Davydov 522

Framboidal vaterite aggregates and their transformation into calcite: A morphological study
G. Nehrke and P. Van Cappellen 528

The 12th US Workshop on Organometallic Vapor Phase Epitaxy

Preface
R. Bhat and C. Caneau 531

Section I: Antimonides

Optical and electrical characterization of OMVPE-grown AlGaAsSb epitaxial layers on InP substrates
T.S. Rao, M.G. So, W.Y. Jiang, T. Mayer, S. Roorda, S.C. Gujrathi, M.L.W. Thewalt, C.R. Bolognesi and S.P. Watkins 532

Improved structure and performance of the GaAsSb/InP interface in a resonant tunneling diode
Z. Kollonitsch, H.-J. Schimper, U. Seidel, K. Möller, S. Neumann, F.-J. Tegude, F. Willig and T. Hannappel 536

Microstructure of ordered nanodomains induced by Bi surfactant in OMVPE-grown GaAsSb
W.Y. Jiang, J.Q. Liu, X. Zhang, M.L.W. Thewalt, K.L. Kavanagh and S.P. Watkins 541

Metal organic chemical vapor deposition of metaphorphic InAs–GaSb superlattices on (0 0 1) GaAs substrates for mid-IR photodetector applications
X.B. Zhang, J.-H. Ryou, R.D. Dupuis, S. Mou, S.L. Chuang, C. Xu and K.-C. Hsieh 545

MOCVD growth of highly strained 1.3 μm InGaAs:Sb/GaAs vertical cavity surface emitting laser
Y.A. Chang, J.T. Chu, C.T. Ko, H.C. Kuo, C.F. Lin and S.C. Wang 550

Section II: Nitrides

Carrier transport by formation of two-dimensional hole gas in p-type $Al_{0.1}Ga_{0.9}N$/GaN superlattice for AlGaInN-based laser diode
S.-N. Lee, T. Jang, J.K. Son, H.S. Paek, T. Sakong, E. Yoon, O.H. Nam and Y. Park 554

Enhanced optical properties of InGaN MQWs with InGaN underlying layers
J.K. Son, S.N. Lee, T. Sakong, H.S. Paek, O. Nam, Y. Park, J.S. Hwang, J.Y. Kim and Y.H. Cho 558

Properties of III-N MOS structures with low-temperature epitaxially regrown ohmic contacts
Y.N. Saripalli, C. Zeng, J.P. Long, D.W. Barlage, M.A.L. Johnson and D. Braddock 562

Modeling the parasitic chemical reactions of AlGaN organometallic vapor-phase epitaxy
M.E. Coltrin, J.R. Creighton and C.C. Mitchell 566

Emissivity-correcting near-UV pyrometry for group-III nitride OMVPE
J.R. Creighton, D.D. Koleske and C.C. Mitchell 572

Effect of thermal annealing induced by p-type layer growth on blue and green LED performance
W. Lee, J. Limb, J.-H. Ryou, D. Yoo, T. Chung and R.D. Dupuis 577

Quaternary AlInGaN multiple quantum well 368 nm light-emitting diode
T.-C. Wang, H.-C. Kuo, Z.-H. Lee, C.-C. Chuo, M.-Y. Tsai, C.-E. Tsai, T.-D. Lee, T.-C. Lu and J. Chi 582

Growth of Ga- and N- polar gallium nitride layers by metalorganic vapor phase epitaxy on sapphire wafers
R. Collazo, S. Mita, A. Aleksov, R. Schlesser and Z. Sitar 586

Correlation of the structural and ferromagnetic properties of $Ga_{1-x}Mn_xN$ grown by metalorganic chemical vapor deposition
M.H. Kane, M. Strassburg, W.E. Fenwick, A. Asghar, A.M. Payne, S. Gupta, Q. Song, Z.J. Zhang, N. Dietz, C.J. Summers and I.T. Ferguson 591

A nucleation study of group III-nitride multifunctional nanostructures
S. Gupta, H. Kang, M. Strassburg, A. Asghar, M. Kane, W.E. Fenwick, N. Dietz and I.T. Ferguson 596

Effect of V/III ratio in AlN and AlGaN MOVPE
A.V. Lobanova, K.M. Mazaev, R.A. Talalaev, M. Leys, S. Boeykens, K. Cheng and S. Degroote 601

Effects of reactor pressure and residence time on GaN MOVPE growth efficiency
W.V. Lundin, E.E. Zavarin, D.S. Sizov, M.A. Sinitsin, A.F. Tsatsul'nikov, A.V. Kondratyev, E.V. Yakovlev and R.A. Talalaev 605

MOCVD growth of thick AlN and AlGaN superlattice structures on Si substrates
M.A. Mastro, C.R. Eddy Jr., D.K. Gaskill, N.D. Bassim, J. Casey, A. Rosenberg, R.T. Holm, R.L. Henry and M.E. Twigg 610

Section III: Dilute Nitrides

Characteristics of InGaAsN-GaAsSb type-II "W" quantum wells
J.-Y. Yeh, L.J. Mawst, A.A. Khandekar, T.F. Kuech, I. Vurgaftman, J.R. Meyer and N. Tansu 615

Characterization of MOVPE-grown GaInNAs quantum well with multi-barriers by Z-contrast imaging and SIMS
K.S. Kim, T. Kim, Y.J. Park, S.I. Baek, Y.W. Kim, H.D. Sun and M.D. Dawson 620

Characterisation of GaAsN layers grown by MOVPE
C. Pelosi, G. Attolini, M. Bosi, M. Avella, M. Calicchio, N. Musayeva and J. Jimenez 625

Section IV: Arsenides and Phosphides

Highly efficient InGaAs QW vertical external cavity surface emitting lasers emitting at 1060 nm
K.S. Kim, J.R. Yoo, S.M. Lee, S.J. Lim, J.Y. Kim, J.H. Lee, S.H. Cho, T. Kim and Y.J. Park 629

Avoidance of surface-related defects in MOVPE-grown InGaP layers
A. Knauer, P. Krispin, A. Dadgar and M. Weyers 633

In situ determination and control of AlGaInP composition during MOVPE growth
M. Zorn, J.-T. Zettler, A. Knauer and M. Weyers 637

Material studies regarding InP-based high-efficiency solar cells
H.-J. Schimper, Z. Kollonitsch, K. Möller, U. Seidel, U. Bloeck, K. Schwarzburg, F. Willig and T. Hannappel 642

Zn enhancement during surfactant-mediated growth of GaInP and GaP
D.C. Chapman, A.D. Howard and G.B. Stringfellow 647

Section V: Reactors and Reactor Modellling

A new MOVPE reactor for heteroepitaxial GaAs deposition on large-scale Ge substrates
C. Pelosi, G. Attolini, M. Bosi, D. Moscatelli, A. Veneroni and M. Masi 652

On the flow stability in vertical rotating disc MOCVD reactors under a wide range of process parameters
B. Mitrovic, A. Gurary and L. Kadinski 656

Section VI: Selective Area and Patterned Growth

Effect of group V partial pressure on the kinetics of selective area MOVPE for GaAs on (1 0 0) exact and misoriented substrate
H. Song, X. Song, M. Sugiyama, Y. Nakano and Y. Shimogaki 664

Control of abnormal edge growth in selective area MOVPE of InP
M. Sugiyama, N. Waki, Y. Nobumori, H. Song, T. Nakano, T. Arakawa, Y. Nakano and Y. Shimogaki 668

Epitaxial growth of thick GaAs on orientation-patterned wafers for nonlinear optical applications
D.F. Bliss, C. Lynch, D. Weyburne, K. O'Hearn and J.S. Bailey 673

Section VII: Precursors

Exceptionally stable vapor delivery of trimethylindium under intense OMVPE growth conditions
D.V. Shenai-Khatkhate, R.A. Ware, R.L. DiCarlo Jr., R.F. Polcari, C.J. Marsman, E. Woelk and A.G. Keiter 679

Section VIII: Oxides and Slicides

Designing novel organogermanium OMVPE precursors for high-purity germanium films
E. Woelk, D.V. Shenai-Khatkhate, R.L. DiCarlo Jr., A. Amamchyan, M.B. Power, B. Lamare, G. Beaudoin and I. Sagnes 684

Metal-organic chemical vapor deposition of ZnO
M. Pan, W.E. Fenwick, M. Strassburg, N. Li, H. Kang, M.H. Kane, A. Asghar, S. Gupta, R. Varatharajan, J. Nause, N. El-Zein, P. Fabiano, T. Steiner and I. Ferguson 688

Horizontal growth of epitaxial (1 0 0) β-$FeSi_2$ templates by metal–organic chemical vapor deposition
K. Akiyama, S. Kaneko, Y. Hirabayashi, T. Suemasu and H. Funakubo 694

Author Index 698

Subject Index 708

CONTENTS direct

This journal is part of **ContentsDirect,** the ***free*** alerting service which sends tables of contents by e-mail for Elsevier books and journals. You can register for **ContentsDirect** online at: **http://contentsdirect.elsevier.com**

Available online at www.sciencedirect.com
SCIENCE DIRECT®
ELSEVIER
Journal of Crystal Growth 287 (2006) 402–407
JOURNAL OF CRYSTAL GROWTH
www.elsevier.com/locate/jcrysgro

Transition metals in photovoltaic-grade ingot-cast multicrystalline silicon: Assessing the role of impurities in silicon nitride crucible lining material ☆

T. Buonassisi[a], A.A. Istratov[a,*], M.D. Pickett[a], J.-P. Rakotoniaina[b], O. Breitenstein[b], M.A. Marcus[c], S.M. Heald[d], E.R. Weber[a]

[a]*Materials Science Division, Department of Materials Science and Engineering, Lawrence Berkeley National Laboratory, University of California, Berkeley, Building 62-109 (MS 62R0203), 1 Cyclotron Road, Berkeley, CA 94720, USA*
[b]*Max Planck Institute of Microstructure Physics, Halle, Germany*
[c]*Advanced Light Source, Lawrence Berkeley National Laboratory, Berkeley, CA 94720, USA*
[d]*Advanced Photon Source, Argonne National Laboratory, Argonne, IL 60439, USA*

Available online 4 January 2006

Abstract

We assess the contamination potential of crucibles used during directionally solidified multicrystalline silicon (mc-Si) ingot casting for cost-effective solar cell wafer production. Highly sensitive, synchrotron-based analytical microprobe techniques were used to study the distributions, sizes, elemental natures and chemical states of impurity-rich particles in α-Si_3N_4 powder representative of what is used to coat the inside of mc-Si ingot-casting crucibles, as well as the as-grown cast mc-Si material. Correlations between the elemental species, chemical states, particle sizes, relative concentrations and locations of impurities (e.g. Fe, Ti, Ca, Zn, Ni, Cu, N, C) concomitant in α-Si_3N_4 and as-grown mc-Si lead us to conclude that α-Si_3N_4 could be a significant source of contaminants during the ingot-casting mc-Si growth process.
© 2005 Elsevier B.V. All rights reserved.

PACS: 78.70; 61.72; 84.60

Keywords: A1. Defects; A1. Impurities; A2. Directional solidification; B1. Nitrides; B2. Semiconducting silicon; B3. Solar cells

1. Introduction

Recent neutron activation analysis (NAA) studies revealed metal concentrations in ingot-cast multicrystalline silicon (mc-Si) materials as high as 10^{13}–10^{16} cm^{-3} (i.e., in the ppb to ppm range) [1–3]. Subsequent studies [4,5] indicated that the majority of metals are present either in (a) metal silicide nanoprecipitates typically <100 nm in diameter, composed of medium- or fast-diffusing metal species, and present in high spatial densities (especially along structural defects), or (b) larger particles up to several microns in size, often in an oxidized chemical state and/or containing multiple slowly diffusing impurity species, present in low spatial densities. A model was developed [5] to explain the presence of both types of particle in mc-Si—the metal silicide nanoprecipitates form from supersaturated metal atoms dissolved within the melt or the crystal, while the micron-sized particles are likely to be inclusions of foreign particles that enter the melt and are incorporated by the advancing solidification front. Understanding the sources and mechanisms of metal contamination is a vital first step to reduce metal contamination levels in mc-Si solar cells.

In this manuscript, we assess the contamination potential of crucibles used during directionally solidified mc-Si ingot casting (i.e. the technology that currently produces

☆This manuscript corresponds to the invited talk "Transition metals in photovoltaic-grade multicrystalline silicon" by A.A. Istratov, T. Buonassisi and E.R. Weber at ACCGE-16, Si/PV-1 session.

*Corresponding author. Fax: +1 510 486 4995.
E-mail address: istratov@berkeley.edu (A.A. Istratov).

0022-0248/$ - see front matter © 2005 Elsevier B.V. All rights reserved.
doi:10.1016/j.jcrysgro.2005.11.053

over 50% of solar cells worldwide). This source of contamination is important for the casting technology because of the prolonged contact (several tens of hours) between the crucible (usually a fused silica or graphite crucible lined with a silicon nitride coating) and the silicon melt/crystal during ingot production. If impurities are contained within any of the crucible parts, then contamination of the melt or of the cooling ingot may occur, as suggested by previous studies (e.g., Refs. [6–11]).

2. Materials and methods

Two types of material were analyzed in this study: (a) α-Si_3N_4 powder, and (b) as-grown mc-Si wafers produced from cast ingots.

Samples of α-Si_3N_4 powder were obtained from commercial chemical suppliers (Alfa Aesar and Cerac) and from one of our industrial collaborators; the latter material is representative of what is used in industry to coat the insides of mc-Si ingot-casting crucibles. Four types of commercial α-Si_3N_4 powders were analyzed, with vendor-specified purities ranging from 95% to 99.9%, in addition to the industrial sample. Each type of powder was poured into a small satchel of 5 μm-thick clean polymer and then attached to a sample stage. A background scan on an empty polymer satchel revealed no impurity particles above the detection limits, ensuring that the impurity particles detected by μ-XRF indeed originated from the powder samples themselves.

As-grown ingot-cast mc-Si wafers were extracted from near the bottom, middle, top and edges of several ingots grown by different manufacturers. All samples were lightly etched to remove surface contamination before being measured by highly sensitive synchrotron-based techniques. One particular sample that contained a high density of Si_3N_4 and SiC microdefects was cut vertically from the upper 2 cm of a directionally solidified ingot, as described in Ref. [12]. The wafer was then polished down to ~0.25 μm mean surface roughness for study by infrared transmission microscopy. During the final stage of the polishing process, it was noticed that some microdefects were revealed at the surface of the wafer and could be observed by an optical microscope. These "partially unburied" microdefects were selected for microanalysis by synchrotron-based techniques, after a light etching to remove surface contaminants.

Synchrotron-based X-ray fluorescence microscopy (μ-XRF) was used to map distributions of impurity-rich particles, to identify their elemental compositions, and to determine their sizes. Once impurity-rich particles were located by μ-XRF, their chemical states (e.g., oxide vs. silicide) were identified by the X-ray absorption microspectroscopy (μ-XAS) technique. Details of these experimental techniques can be found in Refs. [4,5,13,23].

To perform μ-XRF/XAS measurements, we used beamline 10.3.2 [14] of the Advanced Light Source at Lawrence Berkeley National Laboratory, and beamline 20-ID-B [15] at the Advanced Photon Source of Argonne National Laboratory.

Infrared transmission microscopy (IRTM, performed at MPI Halle) was used to locate Si_3N_4 and SiC microdefects and to observe their structures, which were then correlated to transmission electron microscopy measurements on similar samples to determine their chemical compositions. Energy dispersive X-ray microanalysis (EDX, performed at MPI Halle) confirmed the presence of C and N at these microdefects.

3. Results

3.1. α-Si_3N_4 crucible lining material

The total impurity contents of α-Si_3N_4 powders from commercial suppliers were obtained by inductively coupled plasma optical emission spectroscopy (ICP-OES, performed by the vendors). Fig. 1a shows the results of these analyses, i.e., the most common impurities in α-Si_3N_4. Interestingly, most major impurities, as well as their concentrations, are very similar to those reported [16,17] in α-Si_3N_4 powders studied during the 1970s.

For comparison, Fig. 1b shows impurity content of ingot-cast mc-Si as determined by NAA. Not all elements detected by ICP-OES and plotted in Fig. 1a could be detected in mc-Si by NAA, because NAA is not equally sensitive to all elements [18], and vice versa; hence, the lack of bars in Fig. 1(a) or (b) corresponding to certain elements does not imply that these elements were not present, but

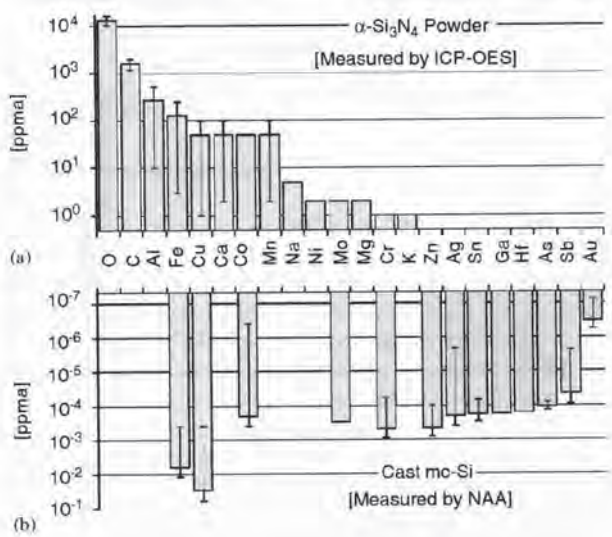

Fig. 1. (a) Vendor-specified impurity contents of four different commercially available α-Si_3N_4 powders with purities between 95% and 99.9%. The range of variation, which depends on the purity of the powder, is shown by the error bars. (b) Impurity content of different directionally solidified ingot-grown mc-Si materials determined by NAA [1–3]. The error bars show the range of values obtained on different samples.

rather means that they could not be detected by a particular analytical technique. The μ-XRF technique, used in our experiments to map distributions of impurities, can easily detect elements such as Fe and Ca, which are some of the most abundant metal impurities, but cannot readily detect lighter elements such as O, N, C and Al, since their fluorescence energies are below 1.5 keV and are strongly absorbed by silicon and air.

Fig. 2 shows a μ-XRF map of Fe and Ca distributions in an α-Si_3N_4 powder provided by our industrial collaborator, and typical of what is used in industry to coat the ingot-casting crucibles. Similar distributions were observed in the powders purchased from commercial vendors. In such powders, iron can be found both distributed homogeneously as well as concentrated in discrete small and large particles. The homogeneously distributed background iron concentration is most readily detectable in lower-purity α-Si_3N_4, and is determined by μ-XAS to be in the $FeSi_2$ chemical state. In addition, discrete Fe-rich particles can be observed in all α-Si_3N_4 materials. The sizes and abundances of these particles decrease with increasing powder purity; the industrial sample demonstrated particle sizes and abundances comparable to the higher-purity commercial samples. These particles exist in two varieties—larger particles of a chemical state most similar to Fe_2O_3 (Fig. 3a), and smaller particles of Fe + Cr + Ni (reminiscent of stainless steel, Fig. 4) with iron in an Fe^0 charge state (such as in iron silicide, metallic iron, iron carbide, etc.) (Fig. 3b). Other less-frequently observed impurity-rich particles contain Cu metal, Zn, Ti, Cr, Ni, Co or Ca. All α-Si_3N_4 powders analyzed in this study exhibit at least two of these types of particle, in addition to the more abundant Fe-rich particles.

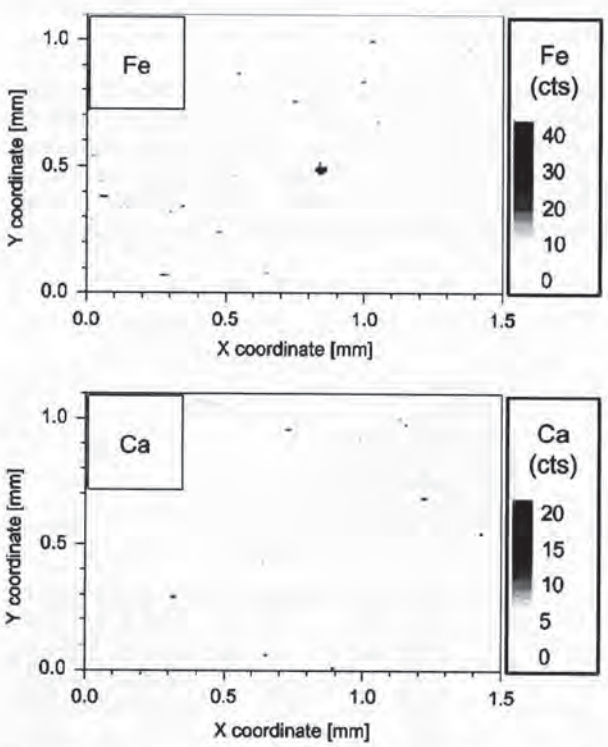

Fig. 2. μ-XRF map of α-Si_3N_4 powder (representative of what is used in industry to coat casting crucibles) reveals the spatial distribution of iron- and calcium-rich particles. Both large and small iron-rich particles are observed. Large Fe-rich particles (such as the one at $X = 0.7$ mm, $Y = 0.5$ mm) contain only iron in a chemical state most similar to Fe_2O_3 (Fig. 3a). The smaller particles consist of Fe + Ni + Cr (Fig. 4), with iron in a Fe^0 charge state, i.e. most similar to metallic Fe (Fig. 3b). Background Fe, detectable in some lower-purity α-Si_3N_4 powders, is determined to be $FeSi_2$. More isolated particles containing Cu metal, Zn, Ti, Cr, Ni and Co were also observed.

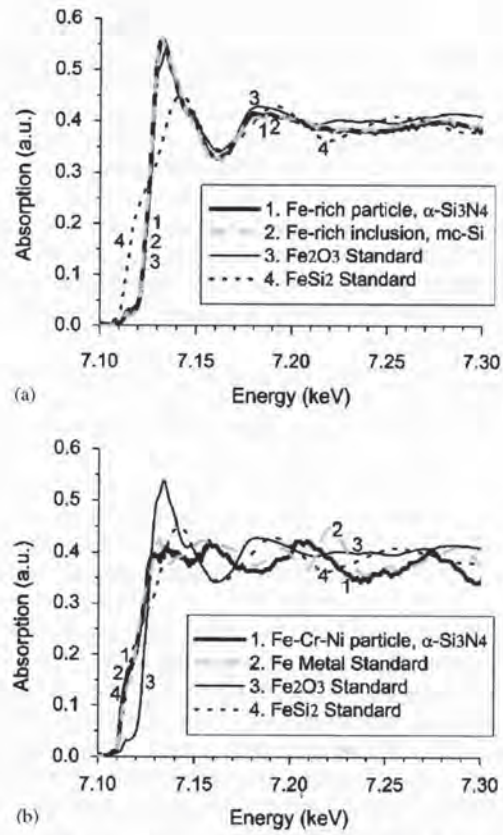

Fig. 3. μ-XAS spectra of two types of Fe-rich particle in α-Si_3N_4 material. The particle in (a) contains a large amount of iron (Fig. 2), and the chemical state is most similar to iron oxide (Fe_2O_3). The particle in (b) consists of Cr, Ni and Fe (Figs. 2 and 4), and the near-edge features match most closely with those of iron in the Fe^0 charge state (e.g. Fe metal, Fe silicide), although the extended X-ray absorption fine spectrum does not match perfectly with any of the standards. Note that the μ-XAS of the oxidized iron particle found in α-Si_3N_4 and that of an oxidized iron inclusion detected in ingot-cast mc-Si material match nearly perfectly, indicating that both the charge state and local crystallographic environment are nearly identical, and providing strong evidence that metal-rich particles in the α-Si_3N_4 crucible lining material can enter the melt during growth.

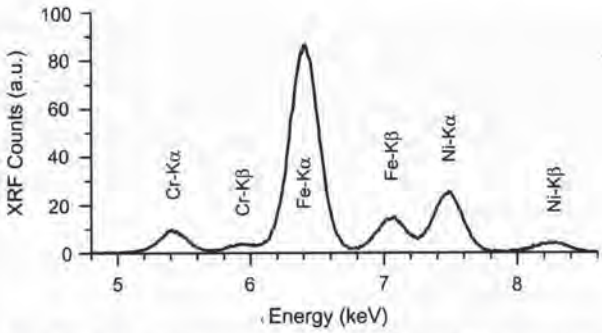

Fig. 4. Typical μ-XRF point spectrum of the smaller Fe-rich particles in Fig. 2. Iron, chromium and nickel are present in proportions suggestive of stainless steel. The μ-XAS spectrum for this particle appears in Fig. 3b.

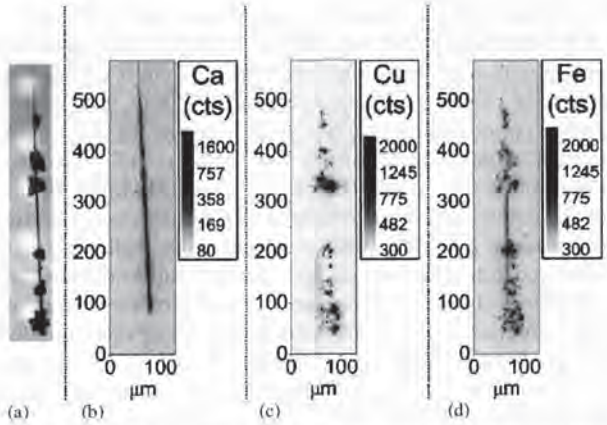

Fig. 5. (a) IRTM image of a β-Si_3N_4 rod encircled by SiC clusters, found in the upper part of a cast mc-Si ingot; (b–d) μ-XRF maps of the same region. Homogeneously distributed Ca and $FeSi_2$ are present at the β-Si_3N_4 rod. Particles of $FeSi_2$ and Cu_3Si are also present at the SiC clusters. All of these impurities are also present in α-Si_3N_4 powder in high concentrations (Figs. 1 and 2).

3.2. Metals in ingot-cast mc-Si

The spatial distributions and chemical states of metal-rich particles in ingot-cast mc-Si turned out to be very similar to those in the silicon nitride coating. In ingot-cast mc-Si, three types of impurity-rich particle are observed by our experimental techniques: (a) metal silicide nanoprecipitates, typically 30–60 nm in diameter, most often found along structural defects (especially grain boundaries), (b) metal-rich inclusions, often measuring up to a few tens of microns in diameter, and (c) extended microdefects (e.g., silicon carbide or nitride) measuring up to several tens or hundred of microns in diameter. Note that the experimental techniques used in this study are insensitive to most metal point defects, such as individual interstitial or substitutional metal atoms.

The metal silicide nanoprecipitates detected in ingot-cast mc-Si are usually found at structural defects (e.g., grain boundaries) and typically contain Ni, Fe, Cu and/or Co, incidentally the 3d transition metal species with highest solubilities and diffusivities in silicon. Further details on structure and properties of metal particles in silicon can be found in our recent publications [4,5,19]. A much higher concentration of these precipitates is observed towards the bottom, top and edges of the ingot. The total amount of metals contained in these precipitates is estimated by μ-XRF to reach values as high as $3 \times 10^{14}\,cm^{-3}$ [5] or higher. On the other hand, in the middle of the ingot, such precipitates are rarely observed above the current μ-XRF detection limits.

Micron-sized particles in mc-Si are often composed of oxidized Fe or Ti (an example of such particle is shown in Ref. [5]). In addition, particles containing Ca, Zn, Mn, Mo and/or Cr, with traces of fast diffusers were also observed. The abundance of slowly diffusing elements, combined with their frequently oxidized chemical state lead us to conclude that these particles are inclusions and not precipitates [4,5]. The spatial density of these particles is orders of magnitude lower than metal silicide nanoprecipitates. However, each inclusion particle contains a far greater number of metal atoms than a metal silicide nanopreciptiate. Consequently, these particles were found to account for local metal contents as high as $2.3 \times 10^{16}\,cm^{-3}$ [5] in regions of the ingot where they are most prevalent (top, bottom and edges).

Metals are also found at Si_3N_4 and SiC microdefects towards the top of the ingot. These microdefects are specific for ingot-cast mc-Si; the significance of finding these microdefects is discussed below. An IRTM image (Fig. 5a) of one collection of microdefects reveals a β-Si_3N_4 rod surrounded by several β-SiC clusters. $FeSi_2$ and Ca (chemical state not determined) are found rather homogeneously distributed within the β-Si_3N_4 rod (Figs. 5b,d), while $FeSi_2$ and Cu_3Si particles are observed within the SiC clusters surrounding the Si_3N_4 rods (Figs. 5(c) and (d)).

4. Discussion and conclusions

The results presented in this study strongly indicate that the silicon nitride coating could contaminate cast mc-Si ingots with an assortment of metallic and non-metallic impurities during crystal growth. Firstly, the *relative concentrations of elemental impurity species* in α-Si_3N_4 are similar to those impurities found in ingot-cast mc-Si, as shown in Fig. 1. It must be noted that the bulk impurity concentrations in the nitride coating and ingot-cast mc-Si wafers were measured using different experimental techniques, each sensitive to a different set of elements (e.g., NAA is not well-suited to detect low-Z elements such as carbon and nitrogen, but it has better sensitivity than ICP-OES to some transition metals). Secondly, the *chemical states* of certain impurity-rich particles in α-Si_3N_4 and inclusions in ingot-cast mc-Si are practically identical, as shown in the overlapping μ-XAS spectra in Fig. 3a. Thirdly, the *distribution* of impurities in ingot-cast mc-Si

ingots suggests an external contamination source in contact with the melt and crystal, given the predominance of precipitates and inclusions near the side edges of ingots. Fourthly, the observation of *silicon nitride and silicon carbide microdefects* in the upper regions of the ingot reflects high concentrations of carbon and nitrogen impurities in the melt. (The precise formation mechanisms of these microdefects is complex and the subject of separate discussions [7,12,20], but it is generally believed that dissolved nitrogen and carbon become supersaturated in the melt during the latter stages of ingot growth, leading to the formation of these microdefects). During directionally solidified cast mc-Si ingot growth, nitride and carbide particles likely decompose from the crucible lining material in contact with the melt. This is consistent with the observation that mc-Si materials not grown in Si_3N_4-coated crucibles seldom exhibit silicon nitride and silicon carbide microdefects, with the exception of silicon carbide microdefects observed in mc-Si materials grown using graphite crucible parts [21] or growth substrates [22]. Upon decomposition of the silicon nitride crucible lining material in contact with the melt, other impurity atoms or particles associated with the nitride can also enter into the melt. This hypothesis is strongly supported by the concomitant presence of N, C, Fe, Ca and Cu at these microdefects (Fig. 5) and within α-Si_3N_4 powders (Figs. 1, 2).

These data suggest two possible mechanisms of incorporating impurities from the crucible lining material coating into mc-Si:

(1) Impurity atoms and impurity-rich particles in the α-Si_3N_4 may dissolve into the silicon melt or warm crystal and form metal point defects, precipitates and/or microdefects. This mechanism likely dominates for small particles (e.g. Fe + Cr + Ni-rich particles), particles with low melting temperatures and impurities distributed atomically or in very small clusters (e.g. background $FeSi_2$ in lower-purity α-Si_3N_4).
(2) Impurity-rich particles in the α-Si_3N_4 may be wholly incorporated into the melt as second-phase particles. If these particles exist for only a short time in the melt, and/or if the melt is already saturated with the given impurity species, then these second-phase particles can be incorporated into the advancing solidification front as inclusions. This is likely to be the case for the relatively large (diameter $\geqslant 1\,\mu m$) oxide-like iron particles occasionally observed in α-Si_3N_4 and near the edges, top, and bottom of mc-Si ingots. It is also possible that certain microdefects are formed this way [7,12,20].

The concentration of impurities in the melt dissolving from the α-Si_3N_4 coating depends on the total thickness of α-Si_3N_4 that dissolves during crystal growth, the elements that may be added during the coating process as sintering aid, as well as on the surface area to volume ratio of the crucible. Effective means of reducing the impact of this contamination source on ingot-cast mc-Si might include reducing the impurity content in α-Si_3N_4, improving the structural quality of Si_3N_4 to minimize its decomposition during growth and reducing the surface area to volume ratio of the crucible (e.g. increasing the crucible size).

Acknowledgments

The beamline assistance of S. Fakra is gratefully acknowledged. M. Werner (MPI Halle) is gratefully acknowledged for supporting discussions of TEM results. This study was supported by NREL subcontract AAT-2-31605-03. T.B. thanks German Academic Exchange Service (DAAD) for a summer research fellowship. The operations of the Advanced Light Source at Lawrence Berkeley National Laboratory are supported by the Director, Office of Science, Office of Basic Energy Sciences, Materials Sciences Division, of the US Department of Energy under Contract no. DEAC03-76SF00098. Use of the Advanced Photon Source was supported by the US Department of Energy, Office of Science, Office of Basic Energy Sciences, under Contract no. W-31-109-ENG-38.

References

[1] A.A. Istratov, T. Buonassisi, R.J. McDonald, A.R. Smith, R. Schindler, J.A. Rand, J.P. Kalejs, E.R. Weber, J. Appl. Phys. 94 (2003) 6552.
[2] D. Macdonald, A. Cuevas, A. Kinomura, Y. Nakano, L.J. Geerligs, J. Appl. Phys. 97 (2005) 33523.
[3] D. Macdonald, A. Cuevas, A. Kinomura, Y. Nakano, in: 29th Photovoltaic Specialists Conference, IEEE, New Orleans, LA, 2002, p. 285.
[4] T. Buonassisi, M.A. Marcus, A.A. Istratov, M. Heuer, T.F. Ciszek, B. Lai, C. Zhonghou, E.R. Weber, J. Appl. Phys. 97 (2005) 63503.
[5] T. Buonassisi, A.A. Istratov, M. Heuer, M.A. Marcus, R. Jonczyk, J. Isenberg, B. Lai, C. Zhonghou, S. Heald, W. Warta, R. Schindler, G. Willeke, E.R. Weber, J. Appl. Phys. 97 (2005) 74901.
[6] S. Binetti, M. Acciarri, C. Savigni, A. Brianza, S. Pizzini, A. Musinu, Mater. Sci. Eng. B 36 (1996) 68.
[7] A.K. Soiland, E.J. Ovrelid, T.A. Engh, O. Lohne, J.K. Tuset, O. Gjerstad, Mater. Sci. Semicond. Process. 7 (2004) 39.
[8] O. Breitenstein, J.P. Rakotoniaina, M.H.A. Rifai, M. Werner, Progr. Photovoltaics: Res. Appl. 12 (2004) 529.
[9] M. Ghosh, D. Yang, A. Lawerenz, S. Riedel, H.J. Möller, in: 14th European Photovoltaic Solar Energy Conference and Exhibition, Barcelona, Spain, 1997, p. 724.
[10] C. Ballif, S. Peters, C. Borchert, C. Hässler, J. Isenberg, R. Schindler, W. Warta, G. Willeke, in: 17th European Photovoltaics Specialists Conference, Munich, Germany, 2001, p. 1818.
[11] M. Rinio, C. Ballif, T. Buonassisi, C. Borchert, in: 19th European Photovoltaic Solar Energy Conference, Paris, France, 2004, p. 762.
[12] J.P. Rakotoniaina, O. Breitenstein, M. Werner, M. Hejjo Al-Rifai, T. Buonassisi, M.D. Pickett, M. Ghosh, A. Müller, N. Le Quang, in: Proceedings of the 20th European Photovoltaic Specialists Conference and Exhibition, Barcelona, Spain, 2005, pp. 773–776.
[13] S.A. McHugo, A.C. Thompson, C. Flink, E.R. Weber, G. Lamble, B. Gunion, A. MacDowell, R. Celestre, H.A. Padmore, Z. Hussain, J. Crystal Growth 210 (2000) 395.
[14] M.A. Marcus, A.A. MacDowell, R. Celestre, A. Manceau, T. Miller, H.A. Padmore, R.E. Sublett, J. Synchrotron Radiat. 11 (2004) 239.

[15] S. Heald, E. Stern, D. Brewe, R. Gordon, D. Crozier, J. Detong, J. Cross, J. Synchrotron Radiat. 8 (2001) 342.
[16] J.L. Iskoe, F.F. Lange, E.S. Diaz, J. Mater. Sci. 11 (1976) 908.
[17] D.P. Elias, M.W. Lindley, J. Mater. Sci. 11 (1976) 1278.
[18] A.R. Smith, R.J. McDonald, H. Manini, D.L. Hurley, E.B. Norman, M.C. Vella, R.W. Odom, J. Electrochem. Soc. 143 (1996) 339.
[19] T. Buonassisi, A.A. Istratov, M.D. Pickett, M. Heuer, J.P. Kalejs, G. Hahn, M.A. Marcus, B. Lai, Z. Cai, S.M. Heald, T.F. Ciszek, R.F. Clark, D.W. Cunningham, A.M. Gabor, R. Jonczyk, S. Narayanan, E. Sauar, E.R. Weber, Progr. Photovoltaics: Res. Appl. (2006) in press.
[20] O. Breitenstein, unpublished, 2005.
[21] J.P. Kalejs, B. Bathey, C. Dube, J. Crystal Growth 109 (1991) 174.
[22] H. Gottschalk, Phys. Stat. Sol. B 222 (2000) 353.
[23] T. Buonassisi, A.A. Istratov, M.A. Marcus, M. Heuer, M.D. Pickett, B. Lai, Z. Cai, S.M. Heald, E.R. Weber, Solid State Phenom. 108–109 (2005) 577.